Edge Transport and its Interconnection with Main Chamber Recycling in ASDEX Upgrade

A. Kallenbach, R. Dux, J. Gafert, G. Haas, L. Horton, M. Jakobi, B. Kurzan, H. W. Müller, R. Neu, J. Neuhauser, R. Pugno, T. Pütterich, V. Rohde, W. Sandmann, S.-W. Yoon and the ASDEX Upgrade team

Max-Planck-Institut für Plasmaphysik, EURATOM Association, D-85748 Garching

e-mail: Arne.Kallenbach@ipp.mpg.de

Abstract. Edge profiles of electron temperature and density are measured in ASDEX Upgrade with high spatial resolution of 2-3 mm with Thomson scattering. In the region of the edge transport barrier in ELMy H-mode, the gradient lengths of T_e and n_e are found closely coupled, with the temperature profile twice as steep as the density profile corresponding to $\eta_e \approx 2$. The edge density in the region of the barrier foot is closely coupled to the main chamber recycling, with no strong dependence on other parameters. In contrast the density rise from the outer barrier foot to the pedestal exhibits pronounced dependence on plasma current and shaping, indicating quite different mechanisms determining the absolute density and its gradient.

1. Introduction

Although the importance of edge transport for power and particle exhaust and its connection to pedestal and core performance have been realised a long time ago, quantitative measurements of temperature and density profiles around the separatrix are sparse for H-mode conditions. The reason is the existence of very steep gradients, which often require a spatial resolution far below 1 cm. The high resolution Thomson scattering system at ASDEX Upgrade provides routinely electron temperature and density measurements in the outer midplane with 2-3 mm spatial resolution. This paper investigates the relation of the edge density profile and main chamber recycling under ELM-averaged H-mode conditions.

2. Edge profile measurements

To obtain high quality edge profiles, Thomson scattering raw data are processed applying Bayesian filtering and a separatrix position correction based on power balance and parallel conductivity [1]. The data are fitted with a modified tanh [2] function (see Fig. 1), which allows the calculation of gradients and stability parameters like $\eta_e = d(\log T_e) / d(\log n_e)$. Analysis of a number of ELMy H-mode discharges reveals that η_e is constant and about 2 from the pedestal top into the hot part of the scrape-off layer ($T_e > 10$ eV) [1] as shown in Fig. 2. This observation supports the hypothesis of close connection of particle and energy transport in the edge transport barrier (ETB) region.

3. Main chamber recycling

The neutral source at the main chamber plasma edge is the sum of several contributions: i) radial ion fluxes towards the wall cause a corresponding local neutral source, ii) neutrals leaking through bypasses of the vessel structure which connect part of the main chamber with the high neutral density region in the divertor, and iii) neutrals travelling from the divertor into the main chamber region via multiple CX and wall collisions. All these processes have in common that they are closely coupled to the edge density driving them, either by radial or parallel ion transport. This produces a collinearity of the neutral fluxes in different regions, which makes it difficult to distinguish the origin of the neutrals observed.

New spectroscopic diagnostics have been installed in ASDEX Upgrade which allow to monitor wall fluxes of hydrogen and carbon at the magnetic high-field side (HFS) and low-field side (LFS). The LFS limiter diagnostic views with 10 lines of sight the top, middle and bottom (see

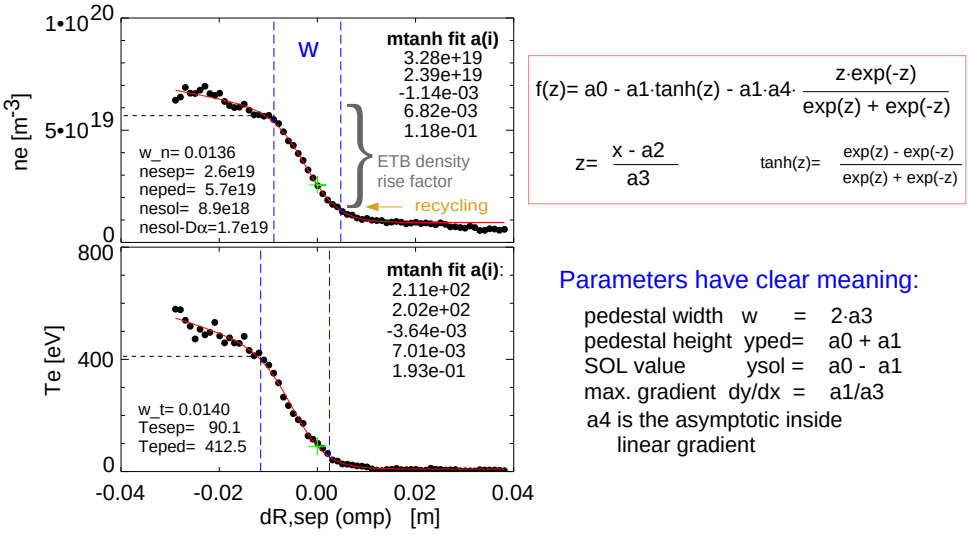

Figure 1: *Edge profiles for a type-I ELMy H-mode from Thomson scattering smoothed with a Bayesian filter. The data are fitted with a modified tanh function, the separatrix position from equilibrium reconstruction is corrected by power balance. # 12200, t=3.4-5.1 s.*

Fig. 3) of 3 out of 12 limiters as well as a toroidally adjacent area with large wall distance. The combined surface area of the LFS limiters is 1 m^2, the 12/3 scaled diagnostic viewing area of 1.3 m^2 is used to obtain the total LFS limiter flux.

A typical recycling distribution along main chamber limiters obtained from Balmer line spectroscopy is indicated in Fig. 3 as well as flux densities and the total influxes from different locations for an outer gap scan and a density scan. As a general finding, the neutral fluxes at all locations correlate very closely. The fluxes on the LFS limiters can be clearly attributed to local plasma flux due to their outstanding recycling intensity compared to regions in the vicinity, but their total contribution is small due to their low surface area. Depending on plasma equilibrium, the top-middle distribution along the limiters varies, limiter-averaged fluxes are considered here. The emission from the inner heat shield rises below the midplane towards the inner divertor and more weakly in upward direction. The highest neutral flux densities occur below the roof baffle in the lower divertor, with values typically 200 (numbers indicated in Fig. 3 vary by a factor 2 for different conditions) times the midplane value (in + out, off limiter). Quite high neutral flux densities (40 times reference value) are measured by ionisation gauges below/behind the HFS heat shield, causing a contribution of bypassing and CX neutrals to the neutral flux in the lower inner heat shield region. The recycling from more remote surfaces and the LFS/HFS distribution are more difficult to quantify since the diagnostic viewing lines pick up the light from both LFS and HFS. Zeeman spectroscopy of the corresponding carbon fluxes show the HFS as the dominant source for viewing lines off the LFS limiters. We assume in the following that 3/4 of the neutral flux along the midplane reference viewing line emerges from the HFS. This value is uncertain, but its effect on the derived total heat shield and limiter fluxes is moderate. Bypass leaking neutral molecules originating from the pump chamber contribute to the main chamber neutral flux on the LFS. The resulting bypass flux is calculated using the conductances derived from experiments with variations of the pumping speed [3] with typical uncertainties $\pm$ 10 m^3/s. The neutrals below the roof baffle reach the pump chamber via the conductance $S_{rb-pump}$= 70 m^3/s. The total pumping speed of S_{pump}= 120 m^3/s and the bypass leak conductance S_{bypass}= 40 m^3/s lead to a significant pressure drop in the pump chamber

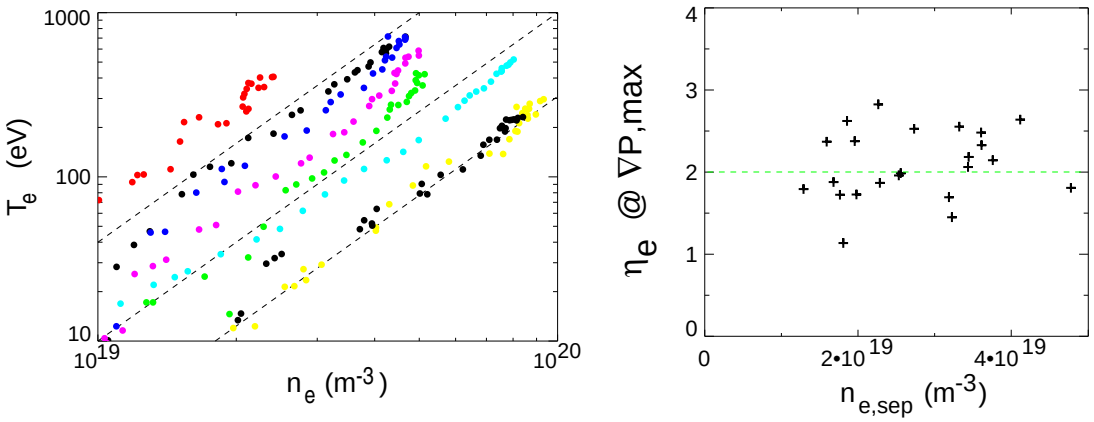

Figure 2: *Electron temperature versus density in the ETB region (- 2cm < dR,sep < 1 cm) for 8 type-I ELMy H-mode discharges. A clear trend $T_e \propto n_e^2$ is observed (dashed lines), which is equivalent to η_e=2. Also shown is η_e calculated from the mtanh fitted profiles at the location of the maximum pressure gradient*

compared to the divertor region below the roof baffle. For a compression ratio f_{comp}= 200 and a contributing plasma surface area of A_{surf}= 20 m^2, the fractional flux density of bypassing neutrals is $f_{by-rec} = \frac{S_{rb-pump} \cdot S_{bypass}}{S_{rb-pump}+S_{pump}+S_{bypass}} \cdot \frac{f_{comp}}{A_{surf}} \frac{1}{v_0}$= 0.38, with v_0= 320 m/s being 1/4 of the thermal molecular speed.

A similar estimate can be done for the bypass neutrals at the lower heat shield: estimating the bypass conductances between roof baffle and lower heat shield and from there towards the plasma to 20 and 80 m^3/s, and allowing 1/3 of the resulting flux to be distributed along the lowest 0.3 m along the heat shield area, an average flux density of 1.6 times the reference value results, or 0.25 times the typical total heat shield flux. In conclusion, bypass neutrals can explain a moderate fraction of the main chamber recycling, the remaining flux is assumed to be caused by ion wall fluxes.

The close correlation of the neutral fluxes in all locations is also valid for variations of the radial plasma position (Fig. 3b) and strong gas puffing (Fig. 3c). Consequently, the total recycling level can be related to the midplane D_α monitor, as done below. In [4], the midplane D_α flux had been connected to an effective SOL density via

$$n_{e,SOL-D\alpha} = 2.7 \cdot 10^9 \, m^{-2} s^{1/2} \; (\Gamma_{D\alpha}[photons \, m^{-2} s^{-1}])^{1/2} \qquad (1)$$

This dependence appeared to be very robust versus experimental parameter variations, the single calibration constant being determined by comparison with SOL averaged profiles from Li-beam measurements. The relatively low neutral influx from the LFS limiters, even for conditions with low LFS wall clearance, is interesting in the context of strong intermittent transport [5]. This is expected to lead to predominantly outward directed ion fluxes on the LFS, which should show up at the well diagnosed LFS limiters. The recycling flux at the LFS limiters is only around 1/5 (see (Fig. 3b+c) of the inner heat shield flux. Therefore, the contribution of intermittent events to the total neutral flux appears to be low.

4. Relation of recycling and density profiles

Edge density profiles and midplane recycling have been evaluated for a number of discharges with good diagnostic coverage. The midplane recycling flux, and namely the effective SOL density $n_{e,SOL-D\alpha}$ derived from the recycling via Eq. 1, can be clearly related to the density

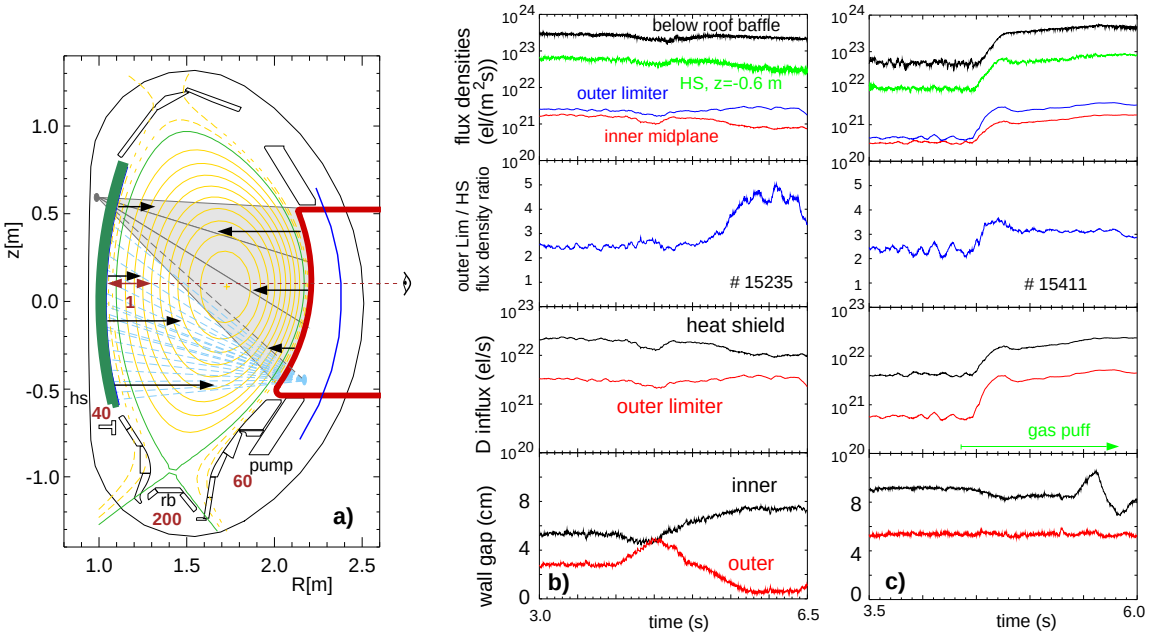

Figure 3: *a) Flux density distribution in the main chamber. The brown double arrow corresponds to the midplane reference recycling D_α monitor measurement using S/XB=20. The black arrows show the local flux densities on the limiter structures. The numbers around the divertor give the relative flux densities measured by ionization gauges. Also shown are the ratios of the outer limiter and midplane inner wall D_α flux densities and the corresponding total fluxes for -0.5 m $< z <$ 0.6 m for a discharge with a pronounced radial sweep (b) and one with a strong gas puff (c). To obtain the total HFS limiter flux, the measured midplane flux density is multiplied with the area of 8.3 m^2 and a profile factor 1.6.*

profile in the SOL, as shown in Fig. 4a. With the choice of calibration factor in Eq. 1, the recycling flux is associated with the electron density at the outer ETB foot. Regression analysis shows the best correlation with the average $(n_{e,sep} \cdot n_{e,SOL})^{0.5}$.
While the SOL density is almost fully interconnected to the neutral recycling, the density rise factor (DRF) over the ETB region, defined here as $\overline{n}_e/n_{e,SOL-D\alpha}$, exhibits a strong dependence on plasma parameters and shape. Using the separatrix T_e from power balance and $n_{e,SOL-D\alpha}$ to calculate the edge normalized Larmor radius, collisionality and beta, the expression for DRF in ASDEX Upgrade and JET was derived [6]:

$$\overline{n}_e/n_{e,SOL-D\alpha} = 32.7\,\nu*^{0.285\pm0.1}\;\rho*^{0.892\pm0.13}\;\beta_t^{-0.796\pm0.1}\;q_{95}^{-0.97\pm0.18}\;(\delta_u+0.2)^{0.372\pm0.06} \quad (2)$$

In dimensional units, this corresponds to a linear I_p dependence. Fig. 4b shows good agreement of the measured DRF with the scaling Eq. 2.

The close correlation of edge density and recycling raises the question of their causality. In fact the causality between these quantities works in both directions, making them interconnected: While the edge density produces neutrals via ion fluxes to the wall (either locally or indirectly via flux amplification in the divertor and neutral transport), the neutrals fuel the plasma in the vicinity of the separatrix. Recent results from DIII-D [7] suggest the neutral penetration depth as a leading parameter for the width of the pedestal. Fig. 4c shows the electron density pedestal and temperature widths obtained from mtanh fitting as a function of line averaged density. Both widths appear very similar on average and show a slight negative trend with density. This trend is much weaker than the inverse density dependence expected from a simple neutral penetration

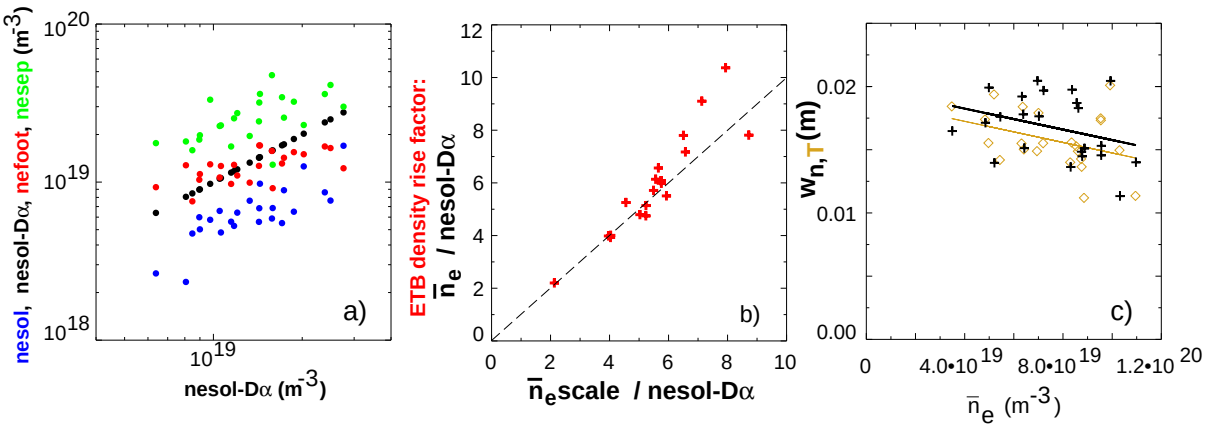

Figure 4: *a) Electron densities at the separatrix, outer density barrier foot and flat SOL density mtanh fit value versus effective SOL density derived from D_α recycling. b) Density rise factor over ETB region in experiment and from the scaling Eq. 2. c) Density and T_e barrier width from mtanh fit at outer midplane versus line-averaged density. Data from Div II and Div IIb.*

model. The combination of the weak density dependence of the pedestal width and the positive dependence of the density rise factor on plasma current and upper triangularity suggests the importance of transport and stability on the density buildup.

5. Conclusions

The analysis of edge T_e and n_e profiles with high spatial resolution and the recycling distribution in ASDEX Upgrade lead to the following picture: Due to the relatively stiff distribution of the fluxes the total neutral influx can be characterised by a single flux monitor situated in the midplane. The SOL density around the ETB foot is closely coupled to the main chamber neutral influx according to Eq. 1. This influx consists of neutrals resulting from radial ion fluxes towards the wall and bypass leaking neutrals. The ion fluxes are supposed to contain the contribution of intermittent events in particular on the LFS, but the contribution of these events to the total main chamber recycling is relatively low.

Starting roughly from the ETB foot position and up to the pedestal top, the relative T_e and n_e profile shapes are constrained by $\eta_e \approx 2$, namely the normalized electron temperature profile gradient length T_e / (dT/dR) having half the value of the density profile. The maximum pressure gradient appears to be limited by stability, following approximately ballooning-related criteria for the pedestal pressure [8]. Due to the coupling of the T_e and n_e gradient lengths via the η_e=2 criterium, the edge profile inside the outer ETB foot can be specified by a limit on the pressure gradient. The major unknown quantity in this picture remains the radial extension of the edge transport barrier.

References

[1] Neuhauser, J. et al., Plasma Phys. Controlled Fusion **44** (2002) 855.
[2] Groebner, R. et al., Nucl. Fusion **41** (2002) 1789.
[3] Neu, R. et al., Plasma Phys. Controlled Fusion **44** (2002) 1021.
[4] Kallenbach, A. et al., Plasma Phys. Controlled Fusion **41** (1999) B177.
[5] Krashenninikov, S., Physics Letters A **283** (2001) 368.
[6] Kallenbach, A. et al., Nuclear Fusion **42** (2002) 1184.
[7] Groebner, R. et al., Physics of Plasmas **9** (2002) 2134.
[8] Suttrop, W. et al., Plasma Phys. Controlled Fusion **42** (2000) A97.